Nanojunctions

DOI: 10.1002/smll.200800788

Reversibly Compressible and Stretchable "Springlike" Polymeric Nanojunctions Between Metal Nanoparticles**

*Kabeer Jasuja, Arthur Thompson, and Vikas Berry**

The ability to control the electronic properties and manipulate the surface chemistries of zero- (0D), one- (1D), and two-dimensional (2D) nanostructures has led to the development of novel nanoscale constructs with a wide range of applications. Over the last decade, molecules with actuating mechanics and unique structural properties have been incorporated between electrode junctions[1,2] to develop memory switches,[3] shuttles,[4–6] and rectifiers.[7,8] In addition, 0D nanoparticles have been used for plasmonic devices,[9] gas detection,[10] and biodevices,[11] 1D nanowires for nanogenerators[12,13] and biosensors,[14] and 2D graphene nanostructures in solar cells[15] and gas sensors.[16] Furthermore, the mobility of nanocomponents has recently brought a new degree of freedom in nanodevice operations using novel nanoelectromechanical systems, such as carbon-nanotube switches,[17] biodevices,[18] gas detectors,[10] touch sensors,[19] elastic membranes,[20] and mechanical gauges.[21] Integrating such mobility of nanoparticles with the elasticity of polymers can produce next-generation springlike electromechanical nanodevices and molecular machines. Herein, we present a study of the electromechanics of an array of gold nanoparticles (GNPs) with springlike nanoscale polymeric junctions incorporated between them.

Integration of the elasticity of polymeric junctions into a device construct requires 1) sustained forces applied to the junction from opposite directions, 2) a structurally well-integrated polymeric junction, and 3) a nonrigid system with reasonable mobility to achieve unrestrained motion. Herein, we consider a device with crosslinked poly(allylamine hydrochloride) (cPAH) molecules sandwiched between 30-nm GNPs (Figure 1). Metal nanoparticles, with their low mass and electronic properties that are sensitively dependent on organic capping[22–24] and interparticle distance,[10,18,19,25,26] are great candidates for both applying confined forces and measuring molecular deformation, while the cPAH provides the elastic polymeric junction. The GNP–cPAH structure is fabricated by a diffusional electrostatic assembly process, in which the thickness of the internanoparticle polymeric nanojunctions can be controlled by the duration of nanoparticle deposition and the degree of crosslinking of cPAH (see Experimental Section).

The devices are prepared on a 1-μm-thick silica substrate with gold electrodes 300 nm thick, 5 μm apart, and 0.7 mm wide (Supporting Information, Figure S1). Devices with high PAH (HP) or low (LP) cPAH junction thickness were fabricated with a GNP deposition time of about 8 and 24 h, respectively (Figure 1a,b). The GNP deposition time determined the deposition density of the GNPs and in turn the thickness of the polymeric junctions (the deposition rate is shown in the Supporting Information, Figure S2). Nanoparticles formed a generally 2D percolating network between gold electrodes (Figure 1c). HP devices were observed to have conductivity an order of magnitude lower than that of LP devices ($d_{HP} > d_{LP}$, Supporting Information, Figure S4). Thermal studies on similar devices[18] have shown that the mode of electron transfer between nanoparticles is electron tunneling[18,27] (direct tunneling at low voltages and Fowler–Nordheim tunneling at higher voltages; Supporting Information, Figure S3). From the Fowler–Nordheim fit to the current–voltage (I–V) curves, the barrier height was calculated to be low (≈0.4 eV) compared to the bandgap of most polymers (6–8 eV), thus invalidating the Fowler–Nordheim fit based on a square barrier.[28] Therefore, in our case, the Fermi level of the metal nanoparticle is close to either the highest occupied molecular orbital (HOMO) or lowest unoccupied molecular orbital (LUMO) level, for which the Simmons model,[29,30] which is based on a triangular barrier, is a more appropriate fit.[28] The barrier heights estimated from the Simmons fit are (0.8335 ± 0.0064) and (0.8156 ± 0.0091) eV for the HP and LP devices, respectively. Further, the difference in the average junction thicknesses of the HP and LP devices is estimated from the Simmons model to be d_{HP}–$d_{LP} = (0.81 \pm 0.007)$ nm (see Experimental Section; error = 0.858%). All the measurements of compression and stretching of junctions reported herein are made by the Simmons model fit, where the conductivity is inverse-exponentially proportional to the barrier width (junction thickness), thus making it sensitively dependent on the junction thickness and giving an accurate estimate of junction compression and stretching.

We present the mechanics of compression and stretching of GNP–cPAH junctions induced by application of a high electric field and a radial centrifugal field, respectively (Figure 1d). To induce compression, a high electric field is applied which polarizes the metal nanoparticles, thus causing a mutual attraction between them.[25] For stretching the junctions, a centrifugal field is applied to induce the nanoparticles to move apart. Further, a solvent-induced GNP rearrangement process is also demonstrated that releases internal stresses in GNP–cPAH structures.

During the electric-field-induced compression process, the electron-tunneling events were found to produce a current of approximately 0.1 μA per nanoparticle or a minimum electron-transport time of $\approx 10^{-12}$ s per nanoparticle. Since a tunneling event has a timescale of the order of 10^{-15} s,[31] during ≈99.9% of the time there is no tunneling and nanoparticles undergo charge polarization which produces

[*] K. Jasuja, A. Thompson, Dr. V. Berry
Department of Chemical Engineering
Kansas State University, KS 66506 (USA)
E-mail: vberry@ksu.edu

[**] V.B. thanks Kansas State University for financial support (Start-up Grant)

Supporting Information is available on the WWW under http://www.small-journal.com or from the author.

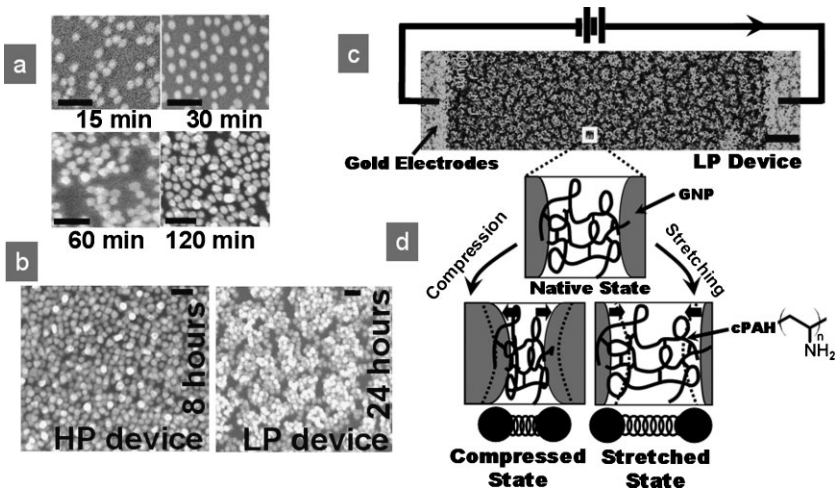

Figure 1. Fabrication and functioning of GNP–cPAH device. a) Field-emission scanning electron microscopy (FESEM) images of 30-nm GNPs deposited on ≈50-nm-thick cPAH film, which show an increase in GNP density with deposition time. Conduction–percolation is achieved at 120 min. b) FESEM images of typical HP and LP devices with deposition times of 8 and 24 h, respectively. c) FESEM image of a typical LP device between gold electrodes connected to a power supply. d) Schematic representation of compression and stretching of cPAH junctions between GNPs. Upon application of a high electric field, the GNPs undergo charge polarization leading to mutual attraction, which compresses the cPAH junction. Upon application of centrifugal force, the GNPs move apart causing the cPAH junctions to stretch. Scale bars: 100 nm for (a,b) and 500 nm for (c).

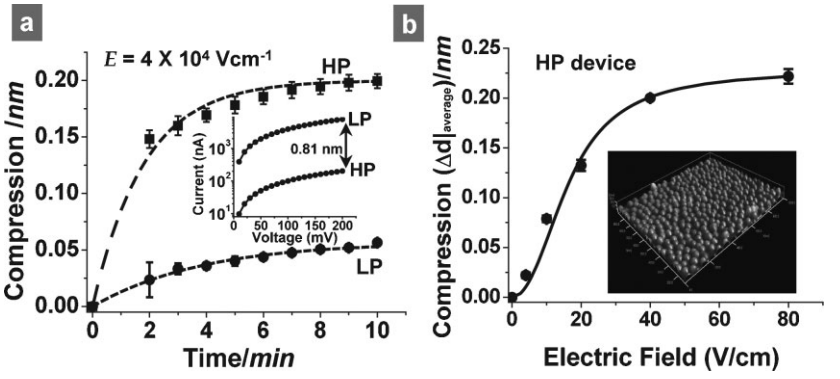

Figure 2. Compression of elastic cPAH junctions. a) Electric-field-induced (4×10^4 V cm^{-1}) cPAH junction compression for LP and HP devices over 10 min, where compression increases with time before reaching a steady-state value of 0.2 and 0.05 nm for the HP and LP devices, respectively. The data fit well with the spring-in-viscous-media equation (dashed line). Inset: native conductivity states for the devices. b) Steady-state junction compression in an HP device as a function of electric field applied for 10 min. The solid line is the fit for compression due to electric-field-induced polarization. Inset: AFM image of an HP device.

the interparticle force. These forces are responsible for the compression process.

Upon application of a 4×10^4 V cm^{-1} electric field for 10 min, the LP and HP devices undergo junction compression that increases with time and reaches a steady-state value of ≈0.05 and ≈0.2 nm, respectively (Figure 2a; see Experimental Section). The rate of molecular compression was found to decrease with time (Supporting Information, Figure S5), thus indicating an increase in opposing force, which is characteristic of a spring (junction). An LP device with lower junction thickness undergoes a lesser compression than an HP device with higher junction thickness (d_{HP}–$d_{LP} = 0.81$ nm; Figure 2a, inset). The average forces per nanoparticle generated by an electric field of 4×10^4 V cm^{-1} were calculated indirectly using the spring constants determined by the centrifugal experiments (shown later). The estimated forces were found to be 1.972×10^{-13} N per junction for the LP device and 6.143×10^{-14} N per junction for the HP device. These values are comparable to the reported force generated by an azo polymer (2.6×10^{-14} N per molecule), where the force from the conformational change of the azo groups led to a 0.22-nm displacement of an attached atomic force microscopy (AFM) tip.[32]

The compression–time curve was found to follow the equation of the spring in viscous media (shown as a dashed line in Figure 2a):

$$\delta^2 \Delta d/\delta t^2 \propto F_{\text{external}} - A\delta \Delta d/\delta t - k\Delta d \quad (1)$$

From this fit, the ratio of the spring constants of the LP and HP devices (k_{LP}/k_{HP}) was found to be 12.32, which is consistent with that calculated from the centrifugal field study (13.18, shown later). This high ratio (k_{LP}/k_{HP}) is expected because the spring constant for axial elongation of a freely jointed chain of a polymer is $k \propto \alpha kT/h^{\beta}$, where h is the extended length of the polymer and α and β ($\beta > 2$) are polymer-specific constants.[33]

The steady-state junction compression was found to increase with the magnitude of the applied electric-field-induced force (Figure 2b). A simple model for the polarization-induced force on the nanoparticles relates the compression to the electric field:

$$E \propto \frac{(\Delta d)^{1/2}\left(1 - \left(\Delta d/d_0\right)\right)}{(1 - B\exp(2.304\Delta d))} \quad (2)$$

where E is the electric field, Δd is the compression, d_0 is the initial average thickness, and B is a constant proportional to the fraction of time tunneling occurs (explained in the Experimental Section). This model fits well with the data (solid line in Figure 2b) with regression of 99.76%. The value of d_{HP} from this fit is (2.34 ± 0.12) nm, which gives a value of $d_{LP} = (1.53 \pm 0.12)$ nm (and d_{HP}–$d_{LP} = 0.81$ nm).

After removing the electric field, the compressed molecules were observed to relax by exerting a force that moves the nanoparticles back to their native positions (Figure 3a). To reduce the timescale of operation, an LP device was initially compressed to a fixed base level, followed by a further

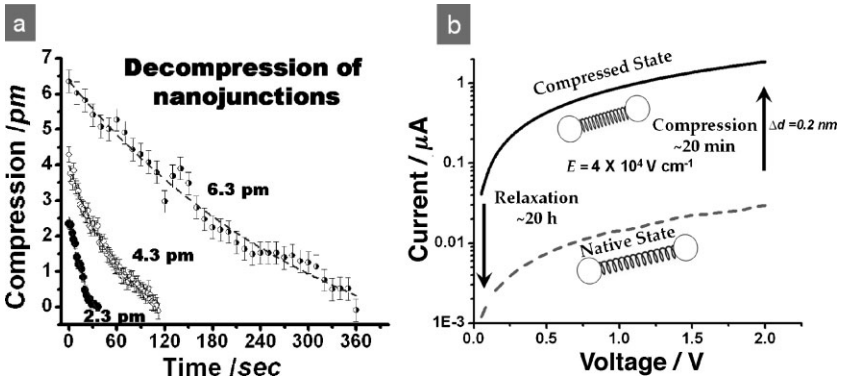

Figure 3. Relaxation of the cPAH junctions. a) Compressed molecules upon release of electric-field-induced forces relax back to their native state with the rate of relaxation governed by the magnitude of compression. An LP device compressed by ≈2.3, 4.3, and 6.3 pm relaxes back to its precompressed state in ≈0.5, 2, and 6 min, respectively. The relaxation data fit well with the spring-in-viscous-media equation (solid line). b) Compression–relaxation cycle of an HP device with two conductivity states. The compressed state (0.2 nm compressed) with conductivity higher by two orders of magnitude is achieved by application of an electric field of 40 kV cm^{-1} for 20 min and the native state is restored after ≈1200 min.

compression of ≈2.3 pm, which decompressed to the base level in ≈0.5 min (Figure 3a). A similar compression by ≈4.3 and 6.3 pm led to decompression to the base level in ≈2 and 6 min, respectively (Figure 3a). The average rate of decompression depends on the thickness of the native junction (Supporting Information, Figure S7) and the magnitude of the induced compression. The rate of decompression followed the spring-in-viscous-media equation (solid line in Figure 3a; see the discussion on device dynamics in the Supporting Information). A complete compression–decompression cycle and the associated two orders of magnitude change in conductivity for the electric-field-induced force on an HP device is shown in Figure 3b, where molecules compressed by 0.2 nm relax back to their native state in ≈1200 min.

Furthermore, since the nanomechanical response of the polymeric junctions depends on the mobility of the GNPs, changing the restraint on the GNPs by anchoring them with different polyelectrolyte thicknesses changes the device performance (Supporting Information, Figure S8). It was determined that for the system to exhibit a reversible compression, the polyelectrolyte thickness cannot be too small (i.e., monolayer) or too large (>100 nm in thickness). For example, devices fabricated through layer-by-layer assembly of $(PAH–GNP)_{10}$, with a monolayer of PAH between the GNPs and the substrate, did not exhibit compression. This finding is attributed to the complete restraining of the GNPs because they are closely bound to the surface. On the other hand, devices fabricated with a much larger polyelectrolyte thickness (>100 nm) exhibited partial relaxation in their initial compression runs (Supporting Information, Figure S9). This result is attributed to an irreversible relocation of GNPs into the larger polyelectrolyte network. Finally, the devices with a ≈50-nm-thick polyelectrolyte layer and 30-nm GNPs show completely reversible compression (Figure 3). Here, the GNPs exhibit a relatively unrestrained mobility without undergoing irreversible relocation. This unrestrained motion also compensates for the collective compression of the junctions (see Supporting Information).

It was established that an electric-field-induced increase in conductivity is a consequence of junction compression and not of charge trapping or ionic conductivity, as explained by the following points. 1) An LP device subjected to successive applications of positive and negative electric fields of 6×10^4 V cm^{-1} for 5 min exhibited a continued increase in conductivity, which indicates a polarization-induced compression (Figure 4a), unlike charge trapping where an increase is expected to be followed by a decrease in conductivity for charging and discharging of the junction. 2) Typically, a two orders of magnitude higher electric field is required for charge trapping than the electric fields used in this study.[34] 3) The conductivity change due to charge trapping occurs at a timescale of micro- to

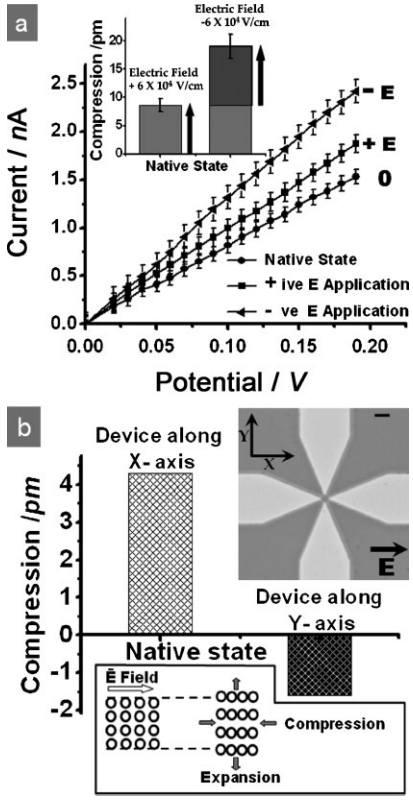

Figure 4. Proof of compression mechanism. a) The conductivity of an HP device increases upon successive applications of electric fields of equal magnitude in the positive ($+6 \times 10^4$ V cm^{-1}) and negative (-6×10^4 V cm^{-1}) directions. Inset: the increase in average junction compression. b) In a crosswire configuration of electrodes, upon application of a 4×10^4 V cm^{-1} electric field in the *x* direction, a molecular compression of ≈4.2 pm along the *x* axis results in molecular stretching of ≈1.8 pm along the *y* axis. Top inset: optical micrograph of the crosswire configuration of electrodes. Bottom inset: schematic of expansion in the *y* direction induced by compression in the *x* direction. (a) and (b) together show that the change in conductivity in LP and HP devices is exclusively a result of molecular compression and not charge trapping. Scale bar: 10 μm.

nanoseconds[35] as a result of fast charge transfer, whereas in this study the timescales are in minutes. 4) There is no diodic behavior or hysteresis for high-voltage *I–V* runs (Supporting Information, Figure S6).

Compression of the molecular junction was confirmed by studying the electromechanical response of a device on a crosswire electrode arrangement (Figure 4b, inset). A 4×10^4 V cm^{-1} electric-field-induced compression of 4.3 pm along the *x* axis resulted in molecular stretching of 1.6 pm in the *y* direction, which indicates transverse-compression-induced longitudinal stretching (Figure 4b). This gives a Poisson's ratio for the GNP–cPAH structure of 0.37, which is comparable to the 0.33 to 0.5 for polyelectrolyte multilayers.[36,37] Since both an increase and a decrease in conductivity are observed instantaneously on the same device, this observation also confirms that the change in conductivity is not a result of the change in contact resistance. Additionally, the conductivity change is not thermally induced since any heat generated due to current flux should dissipate in much smaller timescales; however, in many cases decompression took as long as ≈1000 min. Ionic conductivity was also eliminated as a mode of conduction, since vacuum application led to an increase in conductivity, which is contrary to ionic conductivity.

To induce stretching of the polymeric junctions, a centrifugal field was applied to the GNP–cPAH devices. As expected, all devices under the centrifugal field showed an increase in molecular stretching with time before reaching the steady state (Figure 5a). An LP device placed in a centrifugal field of 90 *g* [≈1.065×10^{-14} N per junction, calculated by using Equation (3)] shows a steady-state molecular stretching of ≈2.7 pm (≈35.61 pm for the HP device; see Supporting Information, Figure S10).

$$F_{\text{centrifugal field}} = (2\pi R \Delta R t \rho_{\text{GNP-cPAH}})\omega^2 \Delta R \quad (3)$$

Here, *R* is the position of the device from the center of the centrifuge, ΔR is the distance between GNPs, ρ and *t* are the density and thickness of the GNP–PAH film, and ω is the angular velocity. As in the case of electric-field-induced compression, the spring-in-viscous-media equation fits well for the centrifugation-induced stretching (solid line in Figure 5a). No cPAH stretching is observed below a threshold centrifugal field of 45 *g*, which corresponds to the static frictional barrier to move nanoparticles (probably due to bonds with the substrate surface). A linear junction stretching is observed above 45 *g*.

A direct measurement of the spring constant (or stiffness) for the HP and LP devices was made by steady-state measurement of stretching at different forces. The spring constant for the HP device was estimated to be $k_{\text{HP}} = 2.99 \times 10^{-4}$ N m^{-1} and for the LP device was $k_{\text{LP}} = 3.94 \times 10^{-3}$ N m^{-1}. The higher spring constant for the LP device is expected, as explained earlier. These values are comparable to the spring constants estimated for lateral compression of polyelectrolyte film ($k = 2.76 \times 10^{-3}$ N m^{-1}).[36] The typical transient relaxation behavior of a device is shown in Figure 5b, where a prestretched LP device, when further stretched by 12 pm, relaxes back to the prestretched level in ≈60 min. The data fit well with the spring-in-viscous-media equation (solid line in Figure 5b). The inset in Figure 5b shows the centrifugation setup. Further, since the deformation of the junctions (electrically measured) is purely mechanically induced by centrifugal force, these results confirm the mechanical characteristics of the junction-deformation model of Figure 1d. However, further microscopic studies will be required to completely understand the mechanism of deformation.

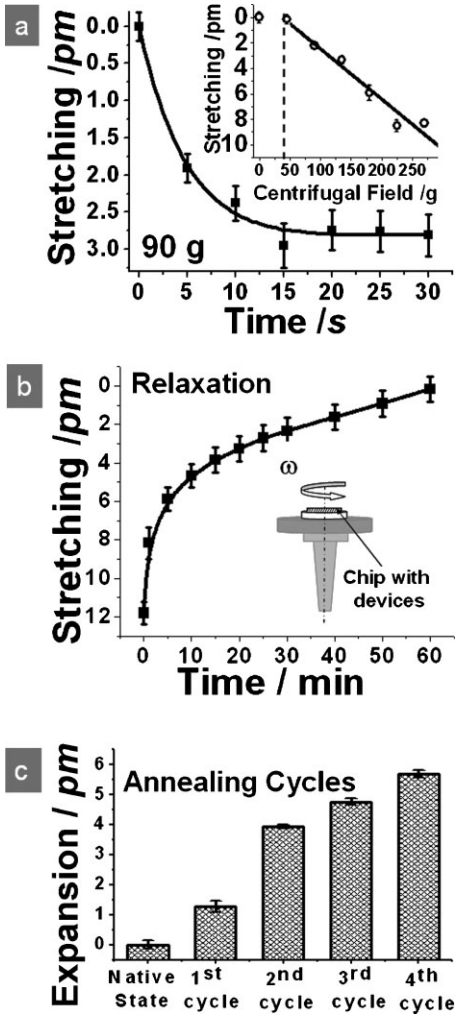

Figure 5. Molecular stretching. a) Centrifugation-induced stretching is achieved by spinning an LP device under a centrifugal field of 90 *g*, which results in an increase in the junction stretching with time. Steady-state stretching of 2.7 pm is achieved in 30 s. The data fit well with the spring-in-viscous-media equation (solid line). The inset shows the increase in stretching with an increase in centrifugal field applied for 30 s. After a threshold centrifugal field of 45 *g*, cPAH junction stretching was found to increase linearly (solid line) with centrifugal field. b) The transient relaxation of another LP device is shown. The device relaxes from its stretched state of 12 pm to its prestretched state in ≈60 min. Inset: schematic of the setup for a device chip on a centrifuge. c) Solvent-induced rearrangement. An LP device annealed with alternate exposures to a vacuum and 40% humidity leads to a decrease in conductivity. After the fourth cycle, an irreversible decrease in conductivity of 13% is achieved, which corresponds to ≈6 pm expansion of the molecular junctions. The observed expansion is expected to be a result of release of internal stress in the GNP–cPAH structure, which was estimated to be 2.36×10^{-14} N per junction.

In another experiment, to release the internal stresses in the nanoparticle array, the GNP–cPAH devices were subjected to multiple annealing cycles of removal and addition of water adsorbed on cPAH junction molecules. An annealing cycle consisted of a 3 min exposure to a vacuum (1 mTorr) to remove the adsorbed water and a 5 min exposure to ≈40% humidity to allow readsorption. A typical response to annealing is shown in Figure 5c, where for an LP device an irreversible increase in average internanoparticle distances of ≈6 pm (corresponding to a decrease in conductivity of the device) was observed after four annealing cycles. This phenomenon is attributed to the release of the internal stresses in the nanoparticle array created during fabrication. While adsorption of water causes cPAH to become charged, mobile, and swollen, desorption of water causes the junction to contract. Repeated cycles of adsorption–desorption allow stabilization and readjustment of the nanoparticles, which causes the release of internal stresses. From our calculations of the spring constant for the LP device, we estimate the internal stresses per nanoparticle due to fabrication to be 2.36×10^{-14} N per junction by using Equation (4):

$$F_{\text{expansion}}/\text{area} = (k_{\text{LP}}x)/(\pi d_{\text{GNP}}^2/4) \quad (4)$$

Finally, it is important to note that the compression–stretching values measured here are the average for the cPAH junctions through which conduction occurs, which in turn are the smallest cPAH layer thicknesses, since conduction occurs through the least-resistant paths. Also, because we used a different set of LP and HP devices on the same chip for electrically induced compression, centrifugally induced stretching, and annealing, we add a further ≈10% error in calculation of the spring constants and forces.

In conclusion, we have demonstrated a working system in which the springlike mechanics of crosslinked molecular junctions have been incorporated as an active element of an electromechanical nanodevice, where forces (per junction) in the range of 10^{-15} to 10^{-13} N were found to produce 2.7 pm to 0.2 nm reversible compression or stretching of the junctions. The compression and stretching mechanics were found to be sensitively dependent on the junction properties and followed the spring-in-viscous-media model. The spring constants for the junctions were found to be 3.944×10^{-3} and 2.99×10^{-4} N m^{-1} for devices with average junction thicknesses of 1.55 and 2.34 nm, respectively. We envision that this system will provide a solid step forward towards controlled electromechanics of nanoparticle devices. The integration of springlike molecular mechanics within nanodevices, as demonstrated here, can potentially be applied to build next-generation molecular systems, such as molecular-manipulation tools, electromechanical switches, and molecular-energy storage systems, and will add to the evolution of molecular machines and functional nanoelectronics.

Experimental Section

Diffusional electrostatic assembly process: The silica substrate was treated with an oxygen plasma (600 mTorr, 100 W, 120 s) to clean the surface and to introduce hydrophilic groups. Positively charged polyelectrolyte, poly(allylamine hydrochloride) (PAH) solution (5%), was spin-coated (3000 rpm, 30 s) on the clean silica substrate. The film was then baked in oxygen at 140 °C for 18 h to partially crosslink the PAH and to attach it to silica,[38] whereby increasing the baking time and temperature increased the degree of crosslinking. The excess PAH not bound to the substrate was removed by placing the substrate in deionized water for 1 min and drying in nitrogen. The prepared substrate was then suspended in negatively charged GNP solution to deposit GNPs on the cPAH film, followed by washing with water and drying. GNP deposition led to further crosslinking of the cPAH film.

Estimation of compression–stretching: All the measurements of average compression and stretching of the junctions were conducted by the Simmons model for electron tunneling.[18] The low barrier height (≈0.4 eV) calculated from the Fowler–Nordheim fit suggests that the Simmons model is a more appropriate fit for our case. Fitting the data with the Simmons model gave a barrier height of (0.8156 ± 0.0091) eV for the LP device and (0.8335 ± 0.0064) eV for the HP device. The compression Δd was calculated from the Simmons model by taking the ratio between the final and initial conductivities at low bias (0.2 V):

$$\frac{J}{J_0} = \exp\left(-2\frac{\sqrt{2m\varphi}}{\eta}\Delta d\right) \quad (5)$$

where J is the current density, Δd is the compression of tunneling distance, m is the electron mass, φ is the barrier height, and h ($=2\pi\eta$) is Planck's constant. This expression is similar to direct tunneling. The change in the barrier height due to rearrangement of molecules is expected to be low[39] and was not included in the analysis.

Estimation of the difference in tunneling distances d_{HP}–d_{LP}: The difference between the average initial cPAH thicknesses for LP and HP devices was calculated by manipulating the Simmons model to factor out the barrier thickness from the preexponential term (details in the Supporting Information). For both HP and LP devices, conductivities were measured at $V_1 = 0.01$ V ($V \ll \varphi/e$) and $V_2 = 1$ V ($V \approx \varphi/e$) and the following expression was used to calculate the difference in the thickness between LP and HP polymeric junctions:

$$\frac{(J_1^2/J_2)_{\text{HP}}}{(J_1^2/J_2)_{\text{LP}}} = \exp\left(-\frac{\sqrt{m\varphi}}{\eta}\left(4-\sqrt{2}\right)(d_{\text{HP}} - d_{\text{LP}})\right) \quad (6)$$

The difference in the junction thickness (d_{HP}–d_{LP}) was found to be 0.81 nm.

Relationship between compression forces and the electric field: The electric-field-induced forces generated between the nanoparticles are attributed to electric-field-induced polarization of the GNPs. The polarization charges induced would be directly proportional to the total electric field minus the fraction used to generate currents: $q_{\text{polarization}} \propto (E - \alpha IE)$, where E is the applied electric field, I is the current flowing through the systems, and α is the proportionality constant, which is dependent on the fraction of time tunneling takes place. Since the force of attraction between the nanoparticles is caused by these induced charges,

$F \propto (E - \alpha IE)^2 \Big/ (d_0 - \Delta d)^2$, where F is the force, d_0 is the initial average junction thickness, and Δd is the final compression. Further, we know that at equilibrium $F \propto \Delta d$[20] and the current

$$I \propto \exp\left(-2\frac{\sqrt{2m\varphi}}{\eta}\Delta d\right) = \exp(2.304\Delta d) \quad (7)$$

Combining these equations we get:

$$E \propto \frac{(\Delta d)^{1}/2\left(1 - \left(\Delta d/d_0\right)\right)}{(1 - B\exp(2.304\Delta d))} \quad (8)$$

This expression fits well with the data with a regression of 99.76%. From this analysis the initial thickness of the HP device was found to be 2.34 nm.

Keywords:
junctions · molecular electronics · nanoelectromechanical systems · nanoparticles · polymers

[1] L. Venkataraman, J. E. Klare, C. Nuckolls, M. S. Hybertsen, M. L. Steigerwald, *Nature* **2006**, *442*, 904–907.
[2] T. Dadosh, Y. Gordin, R. Krahne, I. Khivrich, D. Mahalu, V. Frydman, J. Sperling, A. Yacoby, I. Bar-Joseph, *Nature* **2005**, *436*, 677–680.
[3] D. Dulic, S. J. van der Molen, T. Kudernac, H. T. Jonkman, J. J. D. de Jong, T. N. Bowden, J. van Esch, B. L. Feringa, B. J. van Wees, *Phys. Rev. Lett.* **2003**, *91*, 207402.
[4] J. E. Green, J. W. Choi, A. Boukai, Y. Bunimovich, E. Johnston-Halperin, E. Delonno, Y. Luo, B. A. Sheriff, K. Xu, Y. S. Shin, H. R. Tseng, J. F. Stoddart, J. R. Heath, *Nature* **2007**, *445*, 414–417.
[5] A. M. Brouwer, C. Frochot, F. G. Gatti, D. A. Leigh, L. Mottier, F. Paolucci, S. Roffia, G. W. Wurpel, *Science* **2001**, *291*, 2124–2128.
[6] N. Koumura, R. W. J. Zijlstra, R. A. van Delden, N. Harada, B. L. Feringa, *Nature* **1999**, *401*, 152–155.
[7] A. Aviram, M. A. Ratner, *Chem. Phys. Lett.* **1974**, *29*, 277.
[8] S. Yasuda, T. Nakamura, M. Matsumoto, H. Shigekawa, *J. Am. Chem. Soc.* **2003**, *125*, 16430–16433.
[9] J. K. Tang, H. L. Rong, X. C. Li, B. S. Zou, J. R. Li, *ChemPhysChem.* **2007**, *8*, 1611–1614.
[10] F. P. Zamborini, M. C. Leopold, J. F. Hicks, P. J. Kulesza, M. A. Malik, R. W. Murray, *J. Am. Chem. Soc.* **2002**, *124*, 8958–8964.
[11] S. J. Park, T. A. Taton, C. A. Mirkin, *Science* **2002**, *295*, 1503–1506.
[12] Y. F. Lin, J. Song, Y. Ding, S. Y. Lu, Z. L. Wang, *Appl. Phys. Lett.* **2008**, *92*, 022105.
[13] J. H. Song, X. D. Wang, J. Liu, H. B. Liu, Y. L. Li, Z. L. Wang, *Nano Lett.* **2008**, *8*, 203–207.
[14] Y. Cui, Q. Q. Wei, H. K. Park, C. M. Lieber, *Science* **2001**, *293*, 1289–1292.
[15] X. Wang, L. J. Zhi, K. Mullen, *Nano Lett.* **2008**, *8*, 323–327.
[16] F. Schedin, A. K. Geim, S. V. Morozov, E. W. Hill, P. Blake, M. I. Katsnelson, K. S. Novoselov, *Nat. Mater.* **2007**, *6*, 652–655.
[17] J. E. Jang, S. N. Cha, Y. J. Choi, D. J. Kang, T. P. Butler, D. G. Hasko, J. E. Jung, J. M. Kim, G. A. J. Amaratunga, *Nat. Nanotechnol.* **2008**, *3*, 26–30.
[18] V. Berry, R. F. Saraf, *Angew. Chem.* **2005**, *117*, 6626–6631; *Angew. Chem. Int. Ed.* **2005**, *44*, 6668–6673.
[19] V. Maheshwari, R. F. Saraf, *Science* **2006**, *312*, 1501–1504.
[20] K. E. Mueggenburg, X. M. Lin, R. H. Goldsmith, H. M. Jaeger, *Nat. Mater.* **2007**, *6*, 656–660.
[21] J. Herrmann, K. H. Muller, T. Reda, G. R. Baxter, B. Raguse, G. J. J. B. de Groot, R. Chai, M. Roberts, L. Wieczorek, *Appl. Phys. Lett.* **2007**, *91*, 183105.
[22] H. Cai, C. Xu, P. G. He, Y. Z. Fang, *J. Electroanal. Chem.* **2001**, *510*, 78–85.
[23] A. S. Blum, *Nano Lett.* **2004**, *4*, 867–870.
[24] R. P. Andres, J. D. Bielefeld, J. I. Henderson, D. B. Janes, V. R. Kolagunta, C. P. Kubiak, W. J. Mahoney, R. G. Osifchin, *Science* **1996**, *273*, 1690–1693.
[25] V. Berry, S. Rangaswamy, R. F. Saraf, *Nano Lett.* **2004**, *4*, 939–942.
[26] H. Wohltjen, A. W. Snow, *Anal. Chem.* **1998**, *70*, 2856–2859.
[27] K. H. Müller, J. Hermann, B. Raguse, G. R. Baxter, T. Reda, *Phys. Rev. B.* **2008**, *66*, 075417.
[28] W. Y. Wang, T. Lee, M. A. Reed, *J. Phys. Chem. B* **2004**, *108*, 18398–18407.
[29] J. G. Simmons, *J. Appl. Phys.* **1963**, *34*, 1793–1803.
[30] J. G. Simmons, *J. Appl. Phys.* **1964**, *35*, 2655–2658.
[31] K. K. Likharev, *Proc. IEEE* **1999**, *87*, 606–632.
[32] T. Hugel, N. B. Holland, A. Cattani, L. Moroder, M. Seitz, H. E. Gaub, *Science* **2002**, *296*, 1103–1106.
[33] G. W. Slater, Y. Gratton, M. Kenward, L. McCormick, F. Tessier, *Soft Mater.* **2004**, *2*, 155–182.
[34] J.-S. Lee, J. Cho, C. Lee, I. Kim, J. Park, Y.-M. Kim, H. Shin, J. Lee, F. Caruso, *Nat. Nanotechnol.* **2007**, *2*, 790–795.
[35] C. Bauer, G. Boschloo, E. Mukhtar, A. Hagfeldt, *Chem. Phys. Lett.* **2004**, *387*, 176–181.
[36] L. Richert, A. J. Engler, D. E. Discher, C. Picart, *Biomacromolecules* **2004**, *5*, 1908–1916.
[37] A. J. Nolte, M. F. Rubner, R. E. Cohen, *Macromolecules* **2005**, *38*, 5367–5370.
[38] G. A. C. M. Spierings, J. Haisma, F. J. H. M. Vanderkruis, *Philips J. Res.* **1995**, *49*, 139–149.
[39] M. Del Valle, R. Gutierrez, C. Tejedor, G. Cuniberti, *Nat. Nanotechnol.* **2007**, *2*, 176–179.

Received: June 4, 2008
Revised: August 18, 2008
Published online: October 30, 2008

